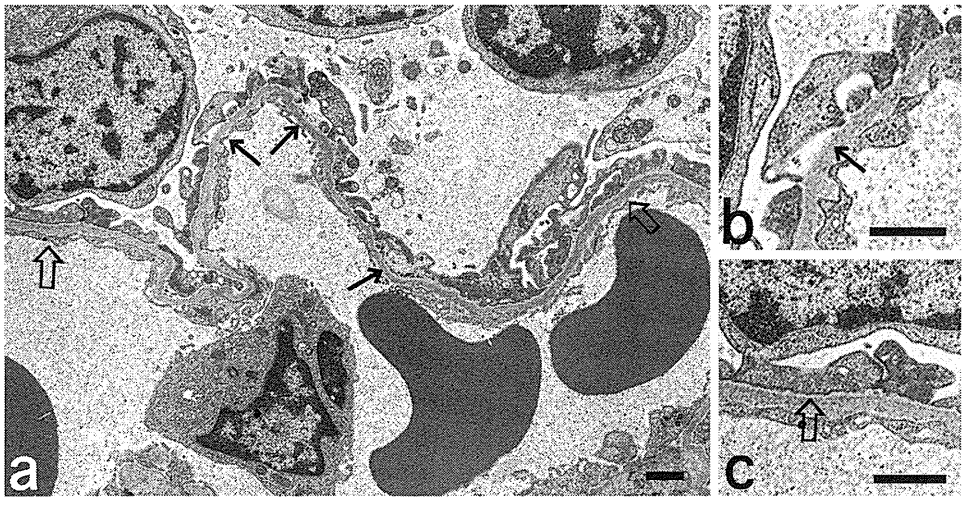

Fig. 7 TEM images of a segment of the glomerular capillary wall in a steroid-resistant NS specimen obtained from the same patient shown in Figure 6b and 6d diagnosed as FSGS. **a)** Irregularities in the thickness and wrinkling of the GBM are clearly observed. Note the detachments (arrows) of podocyte foot processes from the GBM and fusions, effacements, and flattening (open arrows) of the foot processes of podocytes. **b)** A magnified image of the bared GBM (arrow) in (a). **c)** A magnified image of the contacting foot processes (open arrow) in (a). Bars: 1 μm (a, b, c)

ies. Thus, these reports raise the possibility that changes in podocyte cell bodies may be associated with proteinuria. The use of LVSEM is considered to be useful to evaluate NS specimens and to clarify the association between morphological changes in podocytes and proteinuria.

When using LVSEM to evaluate specimens stained with PAM, GBMs were clearly observed, and irregularities in the thickness of GBMs were also detected. Irregularities in thickness and the wrinkling of the GBM were significant findings of the steroid-resistant NS specimens, although these characteristics were not observed in steroid-sensitive NS specimens. These findings may be related to the fact that GBMs in some NS cases were obtained by TEM and that an alteration in the GBM may be a cause of proteinuria. In fact, hematuria and proteinuria are observed in Alport syndrome, a hereditary disorder of the GBM. GBMs were easily and quickly observed in renal paraffin sections using LVSEM, and LVSEM may also be useful to evaluate glomerulopathies caused by alterations in the GBM.

In the present study, we described the morphological differences in glomeruli between steroid-sensitive NS and steroid-resistant NS specimens. The round-shaped podocyte cell bodies were noted especially in steroid-resistant NS specimens, but a semiquantitative analysis of these findings could not be performed because of the small sample sizes. Moreover, the association between the morphological changes of podocytes and the Columbia pathological classification of FSGS was not clarified. Therefore, further studies are required to address these issues.

In conclusion, we considered that the evaluation method of three-dimensional structural alterations in glomerular podocytes and GBMs by LVSEM is probably useful as a novel approach to the histological diagnosis of renal biopsy paraffin sections in pediatric NS.

Acknowledgements

This work was supported by a grant from the Japan Society for the Promotion of Science (a Grant-in-Aid for Scientific Research Number 23591568).

REFERENCES

1. Arakawa M (1971) A scanning electron microscope study of the human glomerulus. *Am J Pathol* **64**, 457–466.
2. Arakawa M and Tokunaga J (1972) A scanning electron microscope study of the glomerulus. Further consideration of the mechanism of the fusion of podocyte terminal processes in nephrotic rats. *Lab Invest* **27**, 366–371.
3. Benzing T (2004) Signaling at the slit diaphragm. *J Am Soc Nephrol* **15**, 1382–1391.
4. Bonsib SM (1984) Scanning electron microscopy of acellular glomeruli in human glomerulonephritis: application of a technique. *Ultrastruct Pathol* **7**, 215–217.
5. Bonsib SM (1985) Glomerular basement membrane discontinuities. Scanning electron microscopic study of acellular glomeruli. *Am J Pathol* **119**, 357–360.
6. Bonsib SM (1985) Scanning electron microscopy of acellular glomeruli in nephrotic syndrome. *Kidney Int* **27**, 678–684.

7. Bonsib SM and Plattner SB (1986) Acellular scanning electron microscopy of spicular renal amyloidosis. *Ultrastruct Pathol* **10**, 497–504.
8. Hidaka S, Oka M, Ito H, Nagase M, Ohta I and Muranaka Y (1990) Gap formation with GBM attenuation as a possible case of glomerular hematuria. *J Clin Electron Microsc* **23**, 5–6.
9. Inaga S, Kato M, Hirashima S, Munemura C, Okada S, Kameie T, Katsumoto T, Nakane H, Tanaka K, Hayashi K and Naguro T (2010/2011) Rapid three-dimensional analysis of renal biopsy sections by low vacuum scanning electron microscopy. *Arch Histol Cytol* **73**, 113–125.
10. Inaga S, Kato M, Hirashima S, Tanaka K, Kameie T, Katsumoto T, Nakane H and Naguro T (2009) Low vacuum scanning electron microscopy of kidney biopsy paraffin sections stained with platinum blue and PAM. *Acta Anat Nippon* **84**, 162 (in Japanese).
11. Jones DB (1977) Correlative scanning and transmission electron microscopy of glomeruli. *Lab Invest* **37**, 569–578.
12. Jones N, Blasutig IM, Eremina V, Ruston JM, Bladt F, Li H, Huang H, Larose L, Li SS, Takano T, Quaggin SE and Pawson T (2006) Nck adaptor proteins link nephrin to the actin cytoskeleton of kidney podocytes. *Nature* **440**, 818–823.
13. Kidney Disease: Improving Global Outcomes (KDIGO) Glomerulonephritis Work Group (2012) KDIGO clinical prectice guideline for glomerulonephritis. *Kidney Int Suppl* **2**, 139–274.
14. Kriz W, Shirato I, Nagata M, LeHir M and Lemley KV (2013) The podocyte's response to stress: the enigma of foot process effacement. *Am J Physiol Renal Physiol* **304**, F333-F347.
15. Kuusniemi AM, Merenmies J, Lahdenkari AT, Holmberg C, Salmela K, Karikoski R, Rapola J and Jalanko H (2006) Glomerular sclerosis in kidneys with congenital nephrotic syndrome (NPHS1). *Kidney Int* **70**, 1423–1431.
16. Lahdenkari AT, Lounatmaa K, Patrakka J, Holmberg C, Wartiovaara J, Kestila M, Koskimies O and Jalanko H (2004) Podocytes are firmly attached to glomerular basement membrane in kidneys with heavy proteinuria. *J Am Soc Nephrol* **15**, 2611–2618.
17. Miyazaki H, Uozaki H, Tojo A, Hirashima S, Inaga S, Sakuma K, Morishita Y and Fukayama M (2012) Application of low-vacuum scanning electron microscopy for renal biopsy specimens. *Pathol Res Pract* **208**, 503–509.
18. Nagata M and Kriz W (1992) Glomerular damage after uninephrectomy in young rats. II. Mechanical stress on podocytes as a pathway to sclerosis. *Kidney Int* **42**, 148–160.
19. Ng W, So KF, So PC and Ngai HK (1982) The preparation of glomeruli from renal biopsy specimens for scanning electron microscopy. *Pathology* **14**, 299–302.
20. Nishimura S, Makino H and Ota Z (1989) Three-dimensional ultrastructural changes of acellular glomerular basement membrane in various types of human glomerulonephritis. *Nephron* **53**, 9–17.
21. Olson JL (2006) The nephrotic syndrome and minimal change disease. In: *Heptinstall's Pathology of the Kidney*, 6th ed (Jennette JC, Olson JL, Schwartz MM, Silva FG, ed.) pp125–154, Lippincott Williams and Wilkins, Philadelphia.
22. Phillips CL, Gattone VH 2nd and Bonsib SM (2006) Imaging glomeruli in renal biopsy specimens. *Nephron Physiol* **103**, 75–81.
23. Rivera A, Magliato S and Meleg-Smith S (2001) Value of electron microscopy in the diagnosis of childhood nephrotic syndrome. *Ultrastruct Pathol* **25**, 313–320.
24. Tarpey PA and Williams G (1980) Scanning electron microscope studies of various glomerulonephropathies. *Med Lab Sci* **37**, 57–80.
25. Tune BM and Mendoza SA (1997) Treatment of the idiopathic nephrotic syndrome: regimens and outcomes in children and adults. *J Am Soc Nephrol* **8**, 824–832.
26. Weidner N and Lorentz WB Jr (1986) Three-dimensional studies of acellular glomerular basement membranes in dense-deposit disease. *Virchows Arch A Pathol Anat Histopathol* **409**, 595–607.
27. Whiteside C, Prutis K, Cameron R and Thompson J (1989) Glomerular epithelial detachment, not reduced charge density, correlates with proteinuria in adriamycin and puromycin nephrosis. *Lab Invest* **61**, 650–660.
28. Yorioka N (1980) Morphological studies on human chronic glomerulonephritis with special reference to grading of glomerular epithelial cell deformities by scanning electron microscopy. *Med J Hiroshima* **28**, 711–764 (in Japanese).
29. Zhang SY, Marlier A, Gribouval O, Gilbert T, Heidet L, Antignac C and Gubler MC (2004) In vivo expression of podocyte slit diaphragm-associated proteins in nephrotic patients with NPHS2 mutation. *Kidney Int* **66**, 945–954.

Biomedical Research (Tokyo) **35** (5) 345-350, 2014

Morphological diagnosis of Alport syndrome and thin basement membrane nephropathy by low vacuum scanning electron microscopy

Shinichi OKADA[1], Sumire INAGA[2], Koichi KITAMOTO[1], Yasuo KAWABA[1], Hironobu NAKANE[2], Tomonori NAGURO[2], Toshiyuki KAIDOH[2], and Susumu KANZAKI[1]

[1] Division of Pediatrics and Perinatology, Faculty of Medicine, Tottori University and [2] Division of Genomic Morphology, Faculty of Medicine, Tottori University

(Received 4 August 2014; and accepted 28 August 2014)

ABSTRACT

Alport syndrome (AS) and thin basement membrane nephropathy (TBMN) are genetic disorders caused by mutations of the type IV collagen genes *COL4A3*, *COL4A4*, and/or *COL4A5*. We here aimed to investigate the three-dimensional ultrastructure of the glomerular basement membrane (GBM) in order to introduce a novel method of diagnosing AS and TBMN. The subjects were 4 patients with AS and 6 patients with TBMN. Conventional renal biopsy paraffin sections from AS and TBMN patients were stained with periodic acid methenamine silver (PAM) and observed directly under low vacuum scanning electron microscopy (LVSEM). The PAM-positive GBMs were clearly visible under LVSEM through the overlying cellular components. The GBMs showed characteristic coarse meshwork appearances in AS, and thin and sheet-like appearances in TBMN. At the cut side view of the capillary wall, the GBMs in AS appeared as fibrous inclusions between a podocyte and an endothelial cell, while the GBMs in TBMN showed thin linear appearances. These different findings of GBMs between AS and TBMN were easily observed under LVSEM. Thus, we conclude that three-dimensional morphological evaluation by LVSEM using conventional renal biopsy paraffin sections will likely be useful for the diagnosis of AS and TBMN, including for retrospective investigations.

Alport syndrome (AS) is a genetic disorder caused by mutations of the type IV collagen genes *COL4A3*, *COL4A4*, and *COL4A5*. It is characterized by renal, cochlear, and ocular involvement, and AS patients are moreover predisposed to developing end-stage renal disease (1, 6, 12). On the other hand, thin basement membrane nephropathy (TBMN) results from mutations of the *COL4A3* and *COL4A4* genes, and is associated with few extra-renal abnormalities and a good renal prognosis. One of the characteristic features of AS and TBMN is morphological changes of the glomerular basement membranes (GBMs). A combination of type IV collagen genes, which produce different constitutions of the alpha chain of collagen type IV, is very important in the construction of normal GBMs. Renal findings under transmission electron microscopy (TEM) of AS include partially thickening, splitting, fragmenting, and basket-weave appearances of the GBMs; whereas TBMN is characterized by a reduction of the thickness of the GBMs. Although the diagnosis of AS or TBMN is generally established by detailed family history, urinalysis, biopsy of the kidney or skin, and molecular genetic analysis, the differential diagnosis is often difficult in both these diseases, owing largely to insufficiency of the biopsy samples and the complexity of molecular genetic analysis. Furthermore, if there are no glomeruli in the biopsy samples for immunofluorescence and TEM analyses,

Address correspondence to: Shinichi Okada, MD, PhD
Division of Pediatrics and Perinatology, Faculty of Medicine, Tottori University
36-1 Nishi-cho, Yonago City, Tottori, Japan
Tel: +81-859-38-6557, Fax: +81-859-38-6559
E-mail: sokada@med.tottori-u.ac.jp

a diagnosis of AS or TBMN can often not be made. Moreover, while AS is generally accompanied by atypical findings of the type IV collagen alpha chains α5 (IV) and α2 (IV) upon immunofluorescence analysis of renal or skin biopsy samples, a mosaic or normal pattern does not always indicate AS or normal findings, respectively. Furthermore, molecular genetic analyses of the type IV collagen genes *COL4A3*, *COL4A4*, and *COL4A5* do not always detect mutations in AS patients (13). Therefore, another efficient and helpful method for diagnosing AS and TBMN is urgently needed.

Adding to the TEM observation of GBM structure, conventional scanning electron microscopy (SEM) of acellular glomeruli in human glomerulonephritis, combined with cell extraction techniques, was developed to visualize the surface structure of the GBM that is present between podocytes and endothelial cells (2, 4). Using this technique, some researchers have investigated GBM alterations in a three-dimensional manner (3, 5, 15, 17); however, to our knowledge, the three-dimensional findings of GBMs in AS or TBMN have not yet been reported.

We have previously demonstrated the usefulness of low vacuum scanning electron microscopy (LVSEM) to evaluate the histological findings of glomeruli by using conventional renal biopsy paraffin sections for the rapid three-dimensional analysis of glomerular structure (10, 14, 16). Especially, the GBMs could be visualized through the overlying cellular components without removal, by staining with periodic acid methenamine silver (PAM) and by using the backscattered electron (BSE) mode of LVSEM, owing to the fact that the PAM stain contains silver, a heavy metal, which enhances the BSE signals. In addition, LVSEM enabled us to investigate intact GBMs without the need for cell lysis, and allows detailed and efficient three-dimensional GBM observation of renal biopsy paraffin specimens more easily than conventional SEM.

In the present study, we investigated the three-dimensional morphological findings of GBMs in AS or TBMN using renal biopsy samples and demonstrate the potential use of LVSEM in the diagnoses of both these diseases.

MATERIALS AND METHODS

A total of 4 (3 males and 1 female) and 6 (1 male and 5 females) patients with AS and TBMN, respectively, were identified. The ages of the patients with AS and TBMN ranged from 3 to 16 years (median age: 12.0 years) and 8 to 19 years (median age: 10.0 years), respectively. All patients received renal biopsies at the Tottori University Hospital under the approval of the Ethics Committee of Tottori University (Permission No. 2107), and were diagnosed by pediatric nephrologists based on the histological results. Paraffin sections of 5 μm in thickness were created from all renal biopsy samples according to the standard procedure, and stained with hematoxylin and eosin (H & E), periodic acid-Schiff, and PAM for light microscopy. The diagnosis of AS or TBMN was confirmed by renal immunofluorescence staining of collagen type IV α5 (IV) and α2 (IV) chains. For immunofluorescence staining, the fresh renal tissue samples were placed into optimal cutting temperature (OCT) compound, snap-frozen in liquid nitrogen, and cut into 4-μm-thick sections from the OCT compound blocks. Direct immunofluorescence staining (11) was performed at the Shigei Medical Research Institute (Okayama, Japan).

The specimens for the LVSEM observation of the GBM structure were prepared as described previously (9, 10). Briefly, renal biopsy paraffin sections of 5 μm in thickness (same as those prepared for light microscopy) were used. The sections on the slides were deparaffinized with xylene and subsequently transferred to distilled water through an alcohol descending series. Next, the sections were stained with PAM but without following H & E staining. After washing with distilled water for 1–2 min, the sections on the slides were directly observed by LVSEM without cover slips. Observations were made with LVSEMs (Hitachi TM-1000 or TM3030; Hitachi Co. Ltd., Tokyo) at an acceleration voltage of 15 kV with 30 Pa. For TEM observation of GBM in some biopsy samples, ultrathin epoxy resin sections were created, stained with uranyl acetate and Pb, and observed using a TEM (Hitachi H-7100; Hitachi Co., Ltd., Tokyo) at an acceleration voltage of 70 kV.

RESULTS

Under LVSEM, the three-dimensional ultrastructure of the GBMs of AS (Fig. 1) and TBMN (Fig. 2) were examined in detail. At the lower magnifications (less than ×1,000), it was difficult to distinguish the differences of the GBMs in the paraffin sections of AS and TBMN (Fig. 1a, Fig. 2a), whereas at higher magnifications, differences in the structure and brightness of the GBMs between AS and TBMN were easily detectable. The GBMs showed characteristic coarse meshwork appearances in AS and thin and sheet-like appearances in TBMN.

Figure 1 shows representative LVSEM and TEM

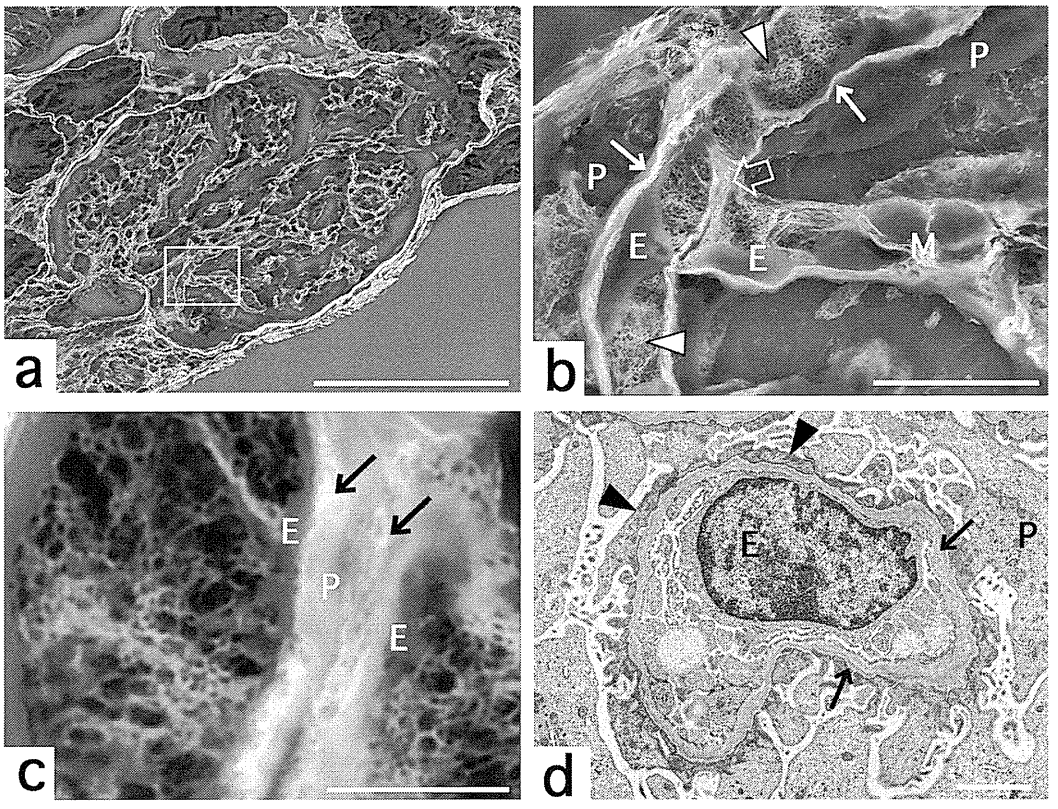

Fig. 1 Electron micrographs of glomerular basement membranes (GBMs) in Alport syndrome (AS) observed by low vacuum scanning electron microscopy (LVSEM) (a–c) and transmission electron microscopy (TEM) (d). (**a**) A glomerulus stained with periodic acid-methenamine-silver (PAM). PAM-positive GBMs, Bowman's basement membrane, and mesangial matrix are recognized at a low magnification (original magnification, ×600). (**b**) A higher-magnification image (×5,000) of the square shown in **a**. The coarse meshwork structure (arrowheads) of the GBMs can be distinctly observed through the thinner parts of the endothelial cells. Conversely, the thick parts of the endothelial cells with nuclei are barely recognized under LVSEM. Irregularities in the thickness of the GBMs can be seen at the cut side of the capillary walls (arrows). (**c**) At the high magnification (×30,000) of the capillary wall (indicated by an open arrow in **b**), the GBMs show distinct three-dimensional basket-weave appearances at the subsurface aspect of the endothelial cells, and fibrous inclusions between the podocytes and endothelial cells can be observed at the cut side view of the GBMs (arrows). (**d**) Under TEM, the GBMs display characteristic basket-weave appearances in AS, with partial thickening, splitting, or fragmenting of the lamina densa (arrows). Focal effacement of the foot processes of the podocytes is also observed (arrowheads). E: endothelial cells, P: podocytes, M: mesangial matrix. Bars: 100 μm (a), 10 μm (b), 2 μm (c, d).

images of glomeruli observed in AS specimens. Positively PAM-stained GBMs, Bowman's basement membrane, and the mesangial matrix of the glomeruli were clearly observed in bright appearances when contrasted to PAM-negative cellular components such as podocytes, endothelial cells, and mesangial cells, which were barely observed under LVSEM (Fig. 1a–c). At higher magnifications (more than ×2,000), LVSEM allowed detailed investigation of the intact subsurface aspects of the capillary walls, which indicated intact GBMs, through the thin parts of the overlying endothelial cells or podocyte foot processes by detecting strong BSE signals from the PAM-positive GBMs (Fig. 1b). The bright GBMs showed irregularities in thickness, and appeared as fibrous inclusions between a podocyte and an endothelial cell at the cut side view of the capillary walls (Fig. 1b, c). The surface appearances of the GBMs observed from the endothelial side showed distinct coarse meshwork structures. Figure 1d shows a TEM image obtained from another AS biopsy sample. In this case, the GBM displayed a basket-weave appearance with partial thickening, splitting, or fragmenting of the lamina densa. The fibrous inclusions or coarse meshwork structures observed under LVSEM were thought to correspond to the lamina densa of the GBMs observed under TEM. Moreover, focal effacements of foot processes of podocytes were also noted.

Figure 2 shows LVSEM and TEM images of glom-

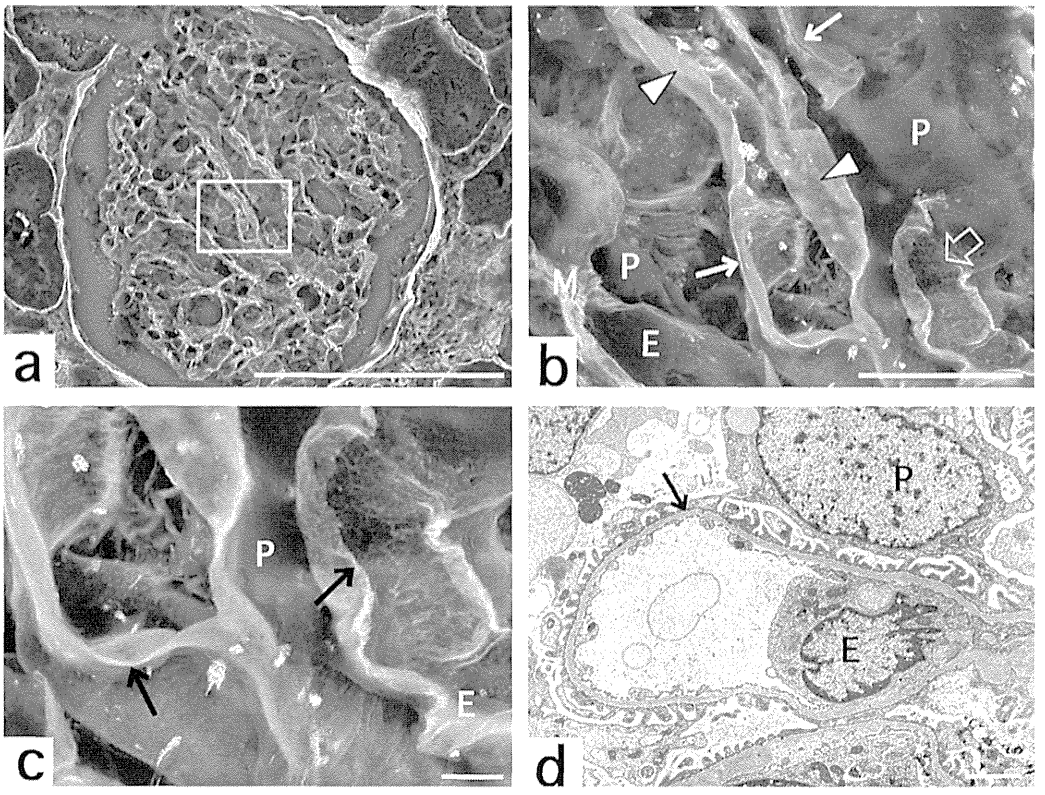

Fig. 2 Electron micrographs of glomerular basement membranes (GBMs) observed in thin basement membrane nephropathy (TBMN) specimens by low vacuum scanning electron microscopy (a–c) and transmission electron microscopy (TEM) (d). (**a**) Periodic acid-methenamine-silver-positive GBMs, Bowman's basement membrane, and mesangial matrix are recognized at a low magnification (×800), similar to in Alport syndrome (AS). (**b**) A higher-magnification image (×5,000) of the square shown in **a**. Widespread thinning (arrows) and sheet-like GBMs (arrowheads) can be noted. The podocytes and endothelial cells of the glomeruli are barely observed. (**c**) A higher-magnification image (×10,000) of the capillary wall (indicated by an open arrow in **b**). The meshwork structure of the GBM is not conspicuous, even at the high magnification, owing to the lower brightness of the GBMs. Unlike the AS specimens, the GBMs of TBMN exhibit thin linear patterns at the cut side view (arrows). (**d**) TEM image of a glomerular capillary wall in TBMN reveals thinning of the GBM (arrow) without splitting or fragmenting of the lamina densa. The foot processes of the podocytes appear normal. E: endothelial cells, P: podocytes, M: mesangial matrix. Bars: 100 μm (a), 10 μm (b), 2 μm (c, d).

eruli obtained from TBMN specimens. The PAM-positive GBMs and Bowman's basement membrane were also recognized at low magnification (Fig. 2a). At higher magnification, widespread thinning of the sheet-like GBMs was noted (Fig. 2b). However, the meshwork structures of the GBMs observed in some parts of the capillary walls were not very conspicuous, even at higher magnifications (Fig. 2b, c), owing to the lower brightness of the GBMs; while the podocytes, endothelial cells, and mesangial cells of the glomeruli were generally obscure. Unlike AS specimens, almost all GBMs in the TBMN specimens exhibited thin linear patterns at the cut side view. The TEM image of the GBMs in TBMN showed widespread reduction in thickness, but no splitting or fragmenting, and the foot processes of the podocytes had normal appearances (Fig. 2d).

DISCUSSION

In this study, we reported on two important findings of AS and TBMN specimens. First, we found that the GBMs of both AS and TBMN specimens were clearly visible under LVSEM through the overlying of other elements, by detecting the BSE signals from PAM-positive GBMs of both the subepithelial and subendothelial sides. Second, we demonstrated that the GBMs in AS specimens under LVSEM showed characteristic coarse meshwork appearances, whereas those in TBMN specimens had thin and sheet-like appearances; and found that the meshwork structures of the GBMs were not conspicuous in TBMN. These different findings of GBMs between AS and TBMN by LVSEM were obvious and easily demonstrated, and were thought to be useful

for the differential diagnoses of these conditions.

The LVSEM revealed the three-dimensional structural features of the GBMs without removing podocytes or endothelial cells. Because the podocytes, endothelial cells, and mesangial cells of the glomeruli were not stained with PAM in the BSE mode of LVSEM, these cellular components showed dark appearances; and the contrasts of the BSE signals between the GBMs and cellular components (podocytes and endothelial cells) contributed to the clear observations of the GBMs in the BSE mode of LVSEM.

Although numerous cross-sectional findings of GBMs in AS under TEM have been reported, reports on the three-dimensional findings of GBMs in AS are rare. GBMs in AS under TEM typically show thickening, splitting, and fragmenting of the lamina densa, with several strands forming a basket-weave pattern (18). In the present study using LVSEM, we found that the GBMs, especially the lamina densa, stained with PAM in AS were distinctly observed in bright appearances, and showed coarse meshwork patterns similar to the TEM findings of the electron-dense lamina. Thus, our results suggest that genetic alterations of collagen type IV in AS lead to three-dimensional morphological changes of collagen type IV in the GBMs, which were shown as a basket-weave pattern under TEM. On the other hand, the three-dimensional morphologies of GBMs in TBMN specimens under LVSEM were distinctly different from those in the AS specimens. The GBMs in TBMN showed thin and sheet-like appearances, unlike the basket-weave pattern observed in AS. These morphological differences of the GBMs can likely be attributed to the genetic differences of collagen type IV between AS and TBMN. Because of the different genetic defects of collagen type IV in AS and TBMN, the GBMs consist of different collagen type IV alpha chains in these disorders, namely α1.α1.α2 (IV) in AS and α3.α4.α5 (IV) in TBMN (8). As different constitutions of alpha chains result in different alterations of the collagen type IV network in GBM (7), this may reflect the different three-dimensional structures of GBMs observed in AS and TBMN. Therefore, the results of the present study suggest that LVSEM is likely useful for the differential diagnoses of AS and TBMN.

However, this study had a number of limitations. Two main issues were that we were unable to assess the correlation between the LVSEM findings of the GBMs and the clinical features of the cases, and that we were unable to evaluate the changes of the glomerular cellular components. Regarding the former issue, analyses of the patient age, sex, hematuria or proteinuria status, and presence of genetic disorders such as X-linked or autosomal recessive or autosomal dominant diseases, could not be performed because of the small sample sizes. Regarding the latter issue, the podocytes and endothelial cells were not estimated because they were PAM-negative elements. Fortunately, we have previously developed the Pt-blue staining method to reveal the morphological changes of glomerular cellular components under LVSEM (10, 16), and we hope that further studies will be performed in the future to address these issues.

In conclusion, the present evaluation method of three-dimensional structural alterations in GBMs by LVSEM using conventional paraffin sections may represent a novel approach to the histological diagnosis of AS and TBMN, including for retrospective investigations. If there are no glomeruli present in the dedicated biopsy sections for immunofluorescence and TEM analyses, the LVSEM method using paraffin sections with sufficient glomeruli could be essential for the diagnosis of AS and TBMN.

Acknowledgements

The authors are grateful to Dr. Ichiro Naito, a former professor in Niimi College, for his valuable suggestions; and Dr. Yoshikazu Sado, Shigei Medical Research Institute, for immunofluorescence of the collagen type IV alpha chains in the renal biopsy specimens. This work was supported by JSPS KAKENHI Grant Number 26461610.

REFERENCES

1. Alport AC (1927) Hereditary familial congenital haemorrhagic nephritis. *Br Med J* **1**, 504–506.
2. Bonsib SM (1984) Scanning electron microscopy of acellular glomeruli in human glomerulonephritis: application of a technique. *Ultrastruct Pathol* **7**, 215–217.
3. Bonsib SM (1985) Glomerular basement membrane discontinuities. Scanning electron microscopic study of acellular glomeruli. *Am J Pathol* **119**, 357–360.
4. Bonsib SM (1985) Scanning electron microscopy of acellular glomeruli in nephrotic syndrome. *Kidney Int* **27**, 678–684.
5. Bonsib SM and Plattner SB (1986) Acellular scanning electron microscopy of spicular renal amyloidosis. *Ultrastruct Pathol* **10**, 497–504.
6. Gubler M, Levy M, Broyer M, Naizot C, Gonzales G, Perrin D and Habib R (1981) Alport's syndrome. A report of 58 cases and a review of the literature. *Am J Med* **70**, 493–505.
7. Gunwar S, Ballester F, Noelken ME, Sado Y, Ninomiya Y and Hudson BG (1998) Glomerular basement membrane. Identification of a novel disulfide-cross-linked network of alpha3, alpha4, and alpha5 chains of type IV collagen and its implications for the pathogenesis of Alport syndrome. *J Biol Chem* **273**, 8767–8775.

8. Hudson BG, Tryggvason K, Sundaramoorthy M and Neilson EG (2003) Alport's syndrome, Goodpasture's syndrome, and type IV collagen. *N Engl J Med* **348**, 2543–2556.
9. Inaga S, Hirashima S, Tanaka K, Katsumoto T, Kameie T, Nakane H and Naguro T (2009) Low vacuum scanning electron microscopy for paraffin sections utilizing the differential stainability of cells and tissues with platinum blue. *Arch Histol Cytol* **72**, 101–106.
10. Inaga S, Kato M, Hirashima S, Munemura C, Okada S, Kameie T, Katsumoto T, Nakane H, Tanaka K, Hayashi K and Naguro T (2010/2011) Rapid three-dimensional analysis of renal biopsy sections by low vacuum scanning electron microscopy. *Arch Histol Cytol* **73**, 113–125.
11. Kagawa M, Kishiro Y, Naito I, Nemoto T, Nakanishi H, Ninomiya Y and Sado Y (1997) Epitope-defined monoclonal antibodies against type-IV collagen for diagnosis of Alport's syndrome. *Nephrol Dial Transplant* **12**, 1238–1241.
12. Kashtan CE and Michael AF (1996) Alport syndrome. *Kidney Int* **50**, 1445–1463.
13. Longo I, Porcedda P, Mari F, Giachino D, Meloni I, Deplano C, Brusco A, Bosio M, Massella L, Lavoratti G, Roccatello D, Frasca G, Mazzucco G, Muda AO, Conti M, Fasciolo F, Arrondel C, Heidet L, Renieri A and De Marchi M (2002) *COL4A3/COL4A4* mutations: from familial hematuria to autosomal-dominant or recessive Alport syndrome. *Kidney Int* **61**, 1947–1956.
14. Miyazaki H, Uozaki H, Tojo A, Hirashima S, Inaga S, Sakuma K, Morishita Y and Fukayama M (2012) Application of low-vacuum scanning electron microscopy for renal biopsy specimens. *Pathol Res Pract* **208**, 503–509.
15. Nishimura S, Makino H and Ota Z (1989) Three-dimensional ultrastructural changes of acellular glomerular basement membrane in various types of human glomerulonephritis. *Nephron* **53**, 9–17.
16. Okada S, Inaga S, Kawaba Y, Hanada T, Hayashi A, Nakane H, Naguro T, Kaidoh T and Kanzaki S (2014) A novel approach to the histological diagnosis of pediatric nephrotic syndrome by low vacuum scanning electron microscopy. *Biomed Res (Tokyo)* **35**, 227–236.
17. Weidner N and Lorentz WB Jr (1986) Three-dimensional studies of acellular glomerular basement membranes in dense-deposit disease. *Virchows Arch A Pathol Anat Histopathol* **409**, 595–607.
18. Yoshikawa N, Ito H, Matsuyama S, Hazikano H, Okada S and Matsuo T (1988) Hereditary nephritis in children with and without characteristic glomerular basement membrane alterations. *Clin Nephrol* **30**, 122–127.

Human Molecular Genetics, 2014, Vol. 23, No. 16 **4345–4356**
doi:10.1093/hmg/ddu152
Advance Access published on April 3, 2014

Distinct pathways leading to TDP-43-induced cellular dysfunctions

Makiko Yamashita[1], Takashi Nonaka[1,*], Shinobu Hirai[2], Akiko Miwa[2], Haruo Okado[2], Tetsuaki Arai[4], Masato Hosokawa[3], Haruhiko Akiyama[3] and Masato Hasegawa[1,*]

[1]Department of Neuropathology and Cell Biology, [2]Department of Brain Development and Neural Regeneration and [3]Dementia Research Project, Tokyo Metropolitan Institute of Medical Science, Tokyo 156-8506, Japan and [4]Department of Neuropsychiatry, Division of Clinical Medicine, Faculty of Medicine, University of Tsukuba, Tsukuba, Ibaraki 305-8575, Japan

Received February 10, 2014; Revised February 10, 2014; Accepted March 31, 2014

TAR DNA-binding protein of 43 kDa (TDP-43) is the major component protein of inclusions found in brains of patients with amyotrophic lateral sclerosis (ALS) and frontotemporal lobar degeneration (FTLD-TDP). However, the molecular mechanisms by which TDP-43 causes neuronal dysfunction and death remain unknown. Here, we report distinct cytotoxic effects of full-length TDP-43 (FL-TDP) and its C-terminal fragment (CTF) in SH-SY5Y cells. When FL-TDP was overexpressed in the cells using a lentiviral system, exogenous TDP-43, like endogenous TDP-43, was expressed mainly in nuclei of cells without any intracellular inclusions. However, these cells showed striking cell death, caspase activation and growth arrest at G2/M phase, indicating that even simple overexpression of TDP-43 induces cellular dysfunctions leading to apoptosis. On the other hand, cells expressing TDP-43 CTF showed cytoplasmic aggregates but without significant cell death, compared with cells expressing FL-TDP. Confocal microscopic analyses revealed that RNA polymerase II (RNA pol II) and several transcription factors, such as specificity protein 1 and cAMP-response-element-binding protein, were co-localized with the aggregates of TDP-43 CTF, suggesting that sequestration of these factors into TDP-43 aggregates caused transcriptional dysregulation. Indeed, accumulation of RNA pol II at TDP-43 inclusions was detected in brains of patients with FTLD-TDP. Furthermore, apoptosis was not observed in affected neurons of FTLD-TDP brains containing phosphorylated and aggregated TDP-43 pathology. Our results suggest that different pathways of TDP-43-induced cellular dysfunction may contribute to the degeneration cascades involved in the onset of ALS and FTLD-TDP.

INTRODUCTION

TAR DNA-binding protein of 43 kDa (TDP-43) has been identified as a major component protein of the ubiquitinated inclusions characteristic of amyotrophic lateral sclerosis (ALS) and frontotemporal lobar degeneration with ubiquitin-positive inclusions (FTLD-U or FTLD-TDP) (1,2). TDP-43 is a ubiquitously expressed nuclear protein and is implicated in exon splicing, gene transcription, regulation of mRNA stability and biosynthesis and formation of nuclear bodies (3–7). It is a 414-amino acid protein with two highly conserved RNA recognition motifs (RRM1 and RRM2) and a glycine-rich region mediating protein–protein interactions at the C-terminus (8–11). In TDP-43 proteinopathy, pathological TDP-43 is abnormally phosphorylated, ubiquitinated and N-terminally cleaved to generate C-terminal fragments (CTFs) (1,12,13).

As autosomal-dominant missense mutations in the *TARDBP* gene were identified in patients with ALS or FTLD-TDP, toxic gain of function of TDP-43 may be related to neuronal degeneration. However, in most cases of TDP-43 proteinopathy, no *TARDBP* mutations are identified, suggesting that wild-type TDP-43 itself is central to the disease cascade. A 2-fold increase in total *TARDBP* mRNA was reported in a 3′-untranslated region variant carrier (14), which suggests that just an increased level of

*To whom correspondence should be addressed at: Department of Neuropathology and Cell Biology, Tokyo Metropolitan Institute of Medical Science, 2-1-6, Kamikitazawa, Setagaya-ku, Tokyo 156-8506, Japan. Tel: +81 36834 2349; Fax: +81 36834 2349; Email: nonaka-tk@igakuken.or.jp (T.N.), hasegawa-ms@igakuken.or.jp (M.H.)

TDP-43 protein (22%) can cause FTLD-TDP. Similarly, overexpression of wild-type TDP-43 causes motor neuron degeneration in yeast, mice and rats (15–17). Moreover, it has recently been reported that the C-terminal portion of TDP-43 shows sequence similarity to prion protein (18) and that truncated CTFs of TDP-43 readily form intracellular aggregates in cultured cells (19–21), suggesting that not only FL-TDP but also its CTFs contribute to the pathogenesis of TDP-43 proteinopathy. However, the molecular mechanisms through which FL-TDP or aggregated CTFs cause neuronal dysfunctions leading to cell death remain unknown. To identify the mechanisms involved, we examined whether overexpression of FL-TDP or its CTF induced cell death in human neuroblastoma line SH-SY5Y cells. We report here that two different pathways lead to cellular dysfunctions induced by FL-TDP and by its CTF. We observed striking apoptotic cell death and cell cycle arrest at the G2/M phase in cells overexpressing FL-TDP. In cells overexpressing TDP-43 CTF, RNA polymerase II (RNA pol II) and several transcription factors such as specificity protein 1 (Sp1) and cAMP-response-element-binding protein (CREB) were co-localized with cytoplasmic aggregates of TDP-43 CTF and their transcriptional activities were decreased, although apoptotic cell death was not significant. These results suggest that recruitment of these factors may cause transcriptional dysregulation, thereby leading to cellular dysfunctions. Dysregulation of FL-TDP expression and/or cytoplasmic accumulation of TDP-43 CTF may contribute to the pathogenesis of ALS and FTLD-TDP.

RESULTS

Overexpression of FL-TDP or its CTF causes cellular dysfunctions in SH-SY5Y cells

Gitcho *et al.* (14) reported a 2-fold increase in total expression of *TARDBP* in a 3′-untranslated region variant carrier of FTLD-TDP, and mice or yeasts overexpressing human TDP-43 develop various abnormalities, including cytotoxicity, neuronal loss and motor deficits (15,17). These findings suggest that overexpression of TDP-43 can cause neuronal degeneration *in vivo*. However, no striking cell death was detected in cultured SH-SY5Y cells transiently expressing a plasmid encoding FL-TDP (20,22). Therefore, to examine whether more substantial and stable expression of TDP-43 is required for induction of its cytotoxic effect in cultured cells, we used a lentiviral system for expression of TDP-43. We prepared SH-SY5Y cells stably expressing FL-TDP (FL-TDP), a deletion mutant of the nuclear localization signal [ΔNLS-TDP; 78–84 residues (23)] and CTF of TDP-43 [C-TDP; 162–414 residues (20)], by using a lentiviral expression system (Fig. 1A). At 3 days after infection, transfected cells were subjected to immunohistochemical and biochemical analyses. Confocal microscopic analyses (Fig. 1B) showed that FL-TDP was expressed mainly in nuclei, but was not phosphorylated or aggregated. ΔNLS-TDP was expressed mainly in cytoplasm, without phosphorylation or aggregation. In cells expressing C-TDP, phosphorylated and aggregated C-TDP was detected with phospho-TDP-43 specific antibody, anti-pS409/410 (Fig. 1B). Immunoblot analyses of transfected cell lysates also revealed that FL-TDP and ΔNLS-TDP were recovered mainly in Triton X-100 (TX)-sup fraction without phosphorylation, while C-TDP was phosphorylated and aggregated in TX-ppt fraction, as shown in Figure 1C.

We examined the cytotoxic effects of these TDP-43 constructs in SH-SY5Y cells. At 4 days after lentiviral infection, the viability of cells transfected with FL-TDP was strongly suppressed and striking cell death was observed (Fig. 2A–C), suggesting that expression of FL-TDP is highly cytotoxic for SH-SY5Y cells. As shown in Figure 2D, poly(ADP-ribose) polymerase (PARP), a well-known substrate for activated caspase-3, was cleaved in cells expressing FL-TDP. This result clearly indicates that expression of FL-TDP induces apoptotic cell death. On the other hand, expression of ΔNLS-TDP or C-TDP did not influence the viability at 4–7 days (Fig. 2B). We also found that expression of the N-terminal fragment of TDP-43 (N-TDP: 1–161 residues) has no cytotoxic effect (Supplementary Material, Fig. S1). In cells expressing C-TDP, however, the number of living cells was significantly less than that in mock cells or cells expressing ΔNLS-TDP at 7 days (Fig. 2C). These results suggest that expression of not only FL-TDP but also CTF of TDP-43 causes cellular dysfunctions in SH-SY5Y cells, and may indicate that expression of FL-TDP without aggregate formation and expression of CTF with inclusions induce cellular damage through distinct mechanisms.

Different modes by which FL-TDP and its CTF induce cellular dysfunctions

To examine this possibility, we performed BrdU incorporation assay in cells expressing green fluorescent protein (GFP)-tagged FL-TDP (GFP-FL-TDP) or CTF (GFP-C-TDP) (Fig. 3A). Since stable expression of TDP-43 using the lentiviral system often resulted in severe damage to SH-SY5Y cells, we mainly used cells transiently expressing TDP-43 plasmids in subsequent work. SH-SY5Y cells were transfected with a plasmid encoding GFP-FL-TDP or GFP-C-TDP for 3 days, then treated with BrdU. After 10 h incubation, the cells were fixed and stained with anti-BrdU antibody and observed with a confocal microscope. As shown in Figure 3B and C, incorporation of BrdU in cells expressing GFP-FL-TDP was significantly decreased when compared with that in cells expressing the empty vector (pEGFP), indicating that DNA synthesis and cell growth were suppressed by overexpression of GFP-FL-TDP. We also found that cells with diffuse expression of GFP-C-TDP were stained with anti-BrdU antibody, while cells including GFP-C-TDP aggregates were not (Fig. 3B, right). Quantitative analysis showed that BrdU incorporation was almost wholly suppressed in cells with GFP-C-TDP inclusions (Fig. 3C). These results indicate that suppression of cell growth owing to formation of GFP-C-TDP inclusions is more marked than that owing to expression of GFP-FL-TDP or GFP-C-TDP without inclusions.

Next, we analyzed the cell cycle by measuring the DNA content of propidium iodide (PI)-stained cells. SH-SY5Y cells were transfected with GFP-FL-TDP or GFP-C-TDP. Three days after transfection, cells were stained with PI and analyzed using a flow cytometer. As shown in Figure 4A and B, cells transfected with GFP-FL-TDP were extensively accumulated in the G2/M and subG1 phases when compared with those transfected with empty vector (pEGFP) or GFP-C-TDP. It is well known that apoptotic cells are accumulated in the subG1 phase, and an increase of cells in the G2/M phase reflects growth arrest, leading to apoptosis. This result shows that overexpression of GFP-FL-TDP induces apoptosis, which is consistent with the